energies

MDPI

Article

Phase Change Materials-Assisted Heat Flux Reduction: Experiment and Numerical Analysis

Hussein J. Akeiber [1,*], Seyed Ehsan Hosseini [1,*], Mazlan A. Wahid [1], Hasanen M. Hussen [2] and Abdulrahman Th. Mohammad [3]

Received: 21 September 2015; Accepted: 25 December 2015; Published: 7 January 2016
Academic Editor: Nyuk Hien Wong

1 High-Speed Reacting Flow Laboratory, Faculty of Mechanical Engineering, Universiti Teknologi Malaysia, 81310 UTM Skudai, Johor 81310, Malaysia; mazlan@fkm.utm.my
2 Machine and Mechanical Department, University of Technology, Baghdad 35023, Iraq; drhasanen_hvac@yahoo.com
3 Baqubah Technical Institute, Middle Technical University, Baghdad 06800, Iraq; abd20091976@gmail.com
* Correspondence: husseinutm@yahoo.com.my (H.J.A.); seyed.ehsan.hosseini@gmail.com (S.E.H.); Tel.: +60-11-1126-1344 (H.J.A.); +60-11-1260-0959 (S.E.H.)

Abstract: Phase change materials (PCM) in the construction industry became attractive because of several interesting attributes, such as thermo-physical parameters, open air atmospheric condition usage, cost and the duty structure requirement. Thermal performance optimization of PCMs in terms of proficient storage of a large amount of heat or cold in a finite volume remains a challenging task. Implementation of PCMs in buildings to achieve thermal comfort for a specific climatic condition in Iraq is our main focus. From this standpoint, the present paper reports the experimental and numerical results on the lowering of heat flux inside a residential building using PCM, which is composed of oil (40%) and wax (60%). This PCM (paraffin), being plentiful and cost-effective, is extracted locally from waste petroleum products in Iraq. Experiments are performed with two rooms of identical internal dimensions in the presence and absence of PCM. A two-dimensional numerical transient heat transfer model is developed and solved using the finite difference method. A relatively simple geometry is chosen to initially verify the numerical solution procedure by incorporating in the computer program two-dimensional elliptic flows. It is demonstrated that the heat flux inside the room containing PCM is remarkably lower than the one devoid of PCM.

Keywords: phase change material (PCM); wax; melting temperature; heat flux

1. Introduction

Over the years, it has been established that thermal energy storage systems (TESSs) with phase change materials (PCMs) can efficiently reduce the excessive usage of fossil fuels and subsequent global warming [1,2]. Thermal energy storage (TES) is found to play a vital role in a broad range of industrial and residential applications. The use of TESSs with PCMs in buildings enhances the human comfort by reducing the internal air temperature fluctuation. Consequently, the indoor air temperature remains near the required temperature over an extended time period [3]. Sensible heat TES, which stores heat in fluid or solid form, latent heat TES, which uses latent heat during the phase change process, and thermoelectric devices are the common examples of different types of TES technologies. TESSs can rapidly discharge or store huge amounts of heat with solar energy and heat as alternating sources [4]. Recent research reveals the advancements of extensive building architecture and management based on TES with PCMs. TES is attractive due to its absolute suitability to reduce the gap between energy demand and supply [5].

Several commercial PCMs have been developed with varying melting temperatures. Considering the cost of various PCMs, Rezaei *et al.* [6] examined their influence on energy and exergy efficiencies. Based on the lumped-parameter method, Li *et al.* [7] established an analytical temperature model. They calculated the enthalpy difference of inorganic salts derived from two types of composite materials. It is shown that the melting point and the enthalpy difference of the binary eutectics ($LiNO_3$-$NaNO_3$, LiCL-NaCL and Li_2CO_3-Na_2CO_3) are consistent with the ones obtained from standard methods. Meanwhile, many efforts are made to produce high performance PCM integration in building walls. Romero-Sanchez *et al.* [8] evaluated the thermal performance of PCMs by incorporating in natural stone. Experiments and numerical simulation are carried out to improve the thermal properties of natural stone, where concrete pilot houses are constructed. These pilot houses are covered with trans-ventilated facade designs via Spanish Bateigazul natural stone. An improvement in human comfort with the reduction in energy consumption is evidenced upon implementing PCMs.

Izquierdo-Barrientos *et al.* [9] inspected the effects of PCMs on external building walls with various configurations by altering the PCMs' layer position, ambient conditions, wall orientation and phase transition temperature. A 1D transient heat transfer numerical model is developed and solved using a finite difference method. Results revealed no significant reduction in the total heat lost during winter irrespective of the variation of the PCM wall orientation or the transition temperature. Moreover, during the summer time, a significant difference in the heat gain is evidenced, which is attributed to the elevated solar radiation fluxes.

The thermal performances of a PCM based co-polymer composite wallboard were experimentally assessed by Kuznik and Virgone [10], where two identical enclosures, called Test Cells 1 and 2, were constructed. The volume of each test cell is (3.10 m × 3.10 m × 2.50 m) and is bounded on five sides by a fixed temperature regulated air mass. The sixth side is a glazed face that separates the test cell from a climate compartment. The air temperature in the room containing PCM is found to decrease up to 4.2 °C without any thermal stratification as compared to the room without PCM composite.

Employing PCM in a representative Mediterranean building, De Gracia *et al.* [11] evaluated its environmental impact in terms of warming. Three scenarios, such as different temperature control systems, different PCM types or different weather conditions, are emphasized based on the life cycle assessment (LCA) process. It is shown that the presence of PCM in the building envelope decreased the energy consumption without considerable reduction of the global impact. The LCA for the real rooms exhibited an impact reduction of 37% upon incorporating polyurethane (PU) into the reference room (REF). Kuznik *et al.* [12] optimized the PCM wallboard thickness in lightweight buildings with reduced air temperature fluctuations inside the room, where the in-house numerical code CODYMUR is used to calculate the optimal thickness.

In another experiment, Navarro *et al.* [13] evaluated the PCM performance in terms of internal thermal gains. Three different rooms with the same internal dimensions (2.4 m × 2.4 m × 2.4 m) are considered. These rooms are labelled as (1) the REF (built using traditional two-layered brick with an air gap and without insulation), (2) the PU (constructed by a traditional brick with of spray foam thickness of 5 cm (walls) and 3 cm (roof)) and (3) the PCM (made with a PCM layer in the southern and western walls and on the roof). It is found that during the summer season the PCM room stored the heat produced by the internal loads, thus limiting the heat dissipation to the outer environment. The REF is found to possess higher temperature fluctuations in its envelope (27.5–24 °C) than other rooms with insulation (28–26 °C).

Pasupathy and Velraj [14] analyzed (theoretically and experimentally) the thermal performance of an inorganic eutectic PCM-based thermal storage system (TSS) for energy conservation in buildings. In the design, one room contained PCM on the roof, and the other room is devoid of the PCM panel. The inner walls, except the ceiling of the rooms, are insulated by a 6 mm-thick plywood on all sides to determine the sole influence of the PCM panel on the roof. The PCM panel is made of (2 m × 2 m) stainless steel having a thickness of 2.54 cm. The stainless steel accommodated an inorganic salt hydrate (48% $CaCl_2$ + 4.3% NaCl + 0.4% KCl + 47.3% H_2O) as the PCM. The measured

room temperatures are observed to vary ~27 $\pm$ 3 °C during the experiment. Despite many dedicated efforts, a comprehensive understanding of the PCM-mediated reduction in heat flux inside the building is far from being achieved.

In this paper, experimental and numerical investigations were performed using PCMs in building architecture to determine their impact on lowering the heat flux inside the building. Two identical rooms, one without and the other with PCM, were considered for experiments. Numerical simulation was done based on the transient heat transfer model. The heat flux inside the room is determined to assess the thermal performance of such PCMs. Results are discussed, analyzed, compared and validated.

2. Numerical Scheme

The boundary condition on the inner surface of the aluminum frame follows natural convection. Most of the previous researchers considered the bottom wall as insulated, because the temperature difference between the room and the wall was very small. The heat transfer coefficient (h) inside the room is calculated (FORTRAN programming). Figures 1 and 2 display the schematics for the numerical model formulation, which assumes the following:

(i) One dimensional heat conduction in the composite wall is considered, and the end impacts are not taken into account.

(ii) The thermal conductivity of the aluminum frame and the roof top slab are constant irrespective of temperature variation.

(iii) The PCM is uniform and isotropic.

(iv) The convection impact in the molten PCM is not considered.

(v) The interfacial resistances are negligible.

(vi) The value of C_p for the PCM panel is considered as follows:

$$T < T_m - \Delta T,\ C_p = C_{ps} \tag{1}$$

$$T > T_m + \Delta T,\ C_p = C_{pl} \tag{2}$$

$$T_m - \Delta T < T < T_m + \Delta T,\ C_p = h_{sl}/2\Delta T \tag{3}$$

where C_p is the specific heat capacity, h_{sl} is the enthalpy change of solid-liquid, ΔT is half of the temperature range over which the phase change occurs and T_m is the phase transition temperature.

(vii) The latent heat being highly sensitive to the phase transition process of the PCM is modeled over a range of temperatures, where C_p is considered to be uniform during the phase conversion. Although, in reality, C_p varies with temperature.

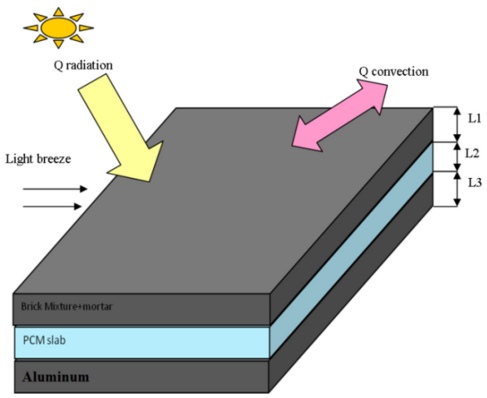

Figure 1. Schematic diagram of phase change material (PCM) incorporated ceiling.

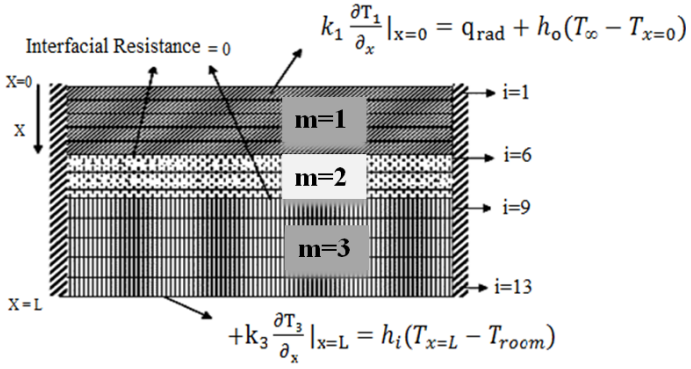

Figure 2. Finite volume grid for the analysis.

Following these assumptions, the governing equation and the boundary conditions are written as:

$$k_{\mathrm{m}} \frac{\partial^2 T_{\mathrm{m}}}{\partial x^2} = \frac{\rho_{\mathrm{m}} C_{\mathrm{pm}} \partial T_{\mathrm{m}}}{\partial t} \{0 < x < L\}; m = 1,2,3 \tag{4}$$

where m = 1 for the roof top slab, m = 2 for the PCM panel and m = 3 for the bottom aluminum frame. The same equation holds for all three material regions and takes different values of k, ρ and C_{p}.

In the outer walls (x = 0), where the floor is exposed to solar radiation, the boundary condition is expressed as:

$$k_1 \frac{\partial T_1}{\partial x}|_{x=0} = q_{\mathrm{rad}} + h_{\mathrm{o}} (T_\infty - T_{x=0}) \tag{5}$$

The radiation effect is considered only during the sunshine hours. The boundary condition ($x = L$) in the bottom layer of the aluminum frame is:

$$k_3 \frac{\partial T_3}{\partial x}|_{x=L} = h_{\mathrm{i}} (T_{x=L} - T_{\mathrm{room}}) \tag{6}$$

The instantaneous continuity of heat flux and temperature at the interfaces $x = L_1$ and L_2 is preserved.

The equation for the top volume cell is written as:

$$\begin{aligned} \left(\frac{\rho_1 c_1 \Delta x_1}{\Delta t} + \frac{f k_1}{\delta x_1} + h_o f\right) T_1 - \frac{f k_1}{\delta x_1} T_2 \\ = h_o f T_\infty + (1-f)\left[\frac{k_1 (T_2 - T_1)}{\delta x_1} - h_o (T_1 - T_\infty)\right] + \frac{\rho_1 c_1 T_1^0}{\Delta t} \Delta x_1 + \alpha q_s \\ + \sigma\left[\alpha T_{\mathrm{sky}}^4 - \in T_{\mathrm{s}}^4\right] \end{aligned} \tag{7}$$

The equation for the volume cells located in between the top and bottom volume cells yields:

$$\begin{aligned} -\frac{f k_{\mathrm{m}}}{\Delta x_{\mathrm{m}}} T_{i+1} + \left[\frac{\rho_{\mathrm{m}} c_{\mathrm{m}} \Delta x_{\mathrm{m}}}{\Delta t} + \frac{f k_{\mathrm{m}}}{\Delta x_{\mathrm{m}}} + \frac{f k_{\mathrm{m}}}{\Delta x_{\mathrm{m}}}\right] T_i - \frac{f k_{\mathrm{m}}}{\Delta x_{\mathrm{m}}} T_i \\ = (1-\mathrm{f})\left[\frac{k_{\mathrm{m}} (T_{i+1} - T_{-i-1})}{\delta x_{\mathrm{m}}} - \frac{k_{\mathrm{m}} (T_i - T_{i-1})}{\delta x_{\mathrm{m}}}\right] + \frac{\rho_{\mathrm{m}} c_{\mathrm{m}} T_{\mathrm{i}}^0 \Delta x_{\mathrm{m}}}{\Delta t} \end{aligned} \tag{8}$$

The above-mentioned discretized equations are applicable to volume cells for 2–4, 7 and for 10–12 of the roof top slab, PCM panel and aluminum frame, respectively, with: m = 1, i = 2, 3, 4; m = 2, i = 7; and m = 3, i =10, 11, 12.

The equation for the interface volume cell 5 is written as:

$$-\frac{fk_1}{\delta x_1}T_4+\left[\frac{\rho_1 c_1\Delta x_1}{\Delta t}+\frac{f}{\delta x_1/2k_1+\delta x_2/2k_2}+\frac{fk_1}{\delta x_1}\right]T_5-\left[\frac{f}{\frac{\Delta x_1}{2k_i}+\frac{\Delta x_2}{2k_2}}\right]T_4 \\ =(1-f)\left[\frac{k_1\left(T_6-T_5\right)}{\delta x_2}-\frac{k_1\left(T_5-T_4\right)}{\delta x_1}\right]+\frac{\rho_1 c_1 T_5^0\Delta x_1}{\Delta t} \tag{9}$$

where Δx_1 and Δx_2 are the cell thickness of the roof top slab and PCM panel, respectively. Similarly, the equation can be written for volume cell 6. A similar process is extended to control Volumes 8 and 9, which involve cell thicknesses Δx_2 and Δx_3 corresponding to the PCM panel and the bottom aluminum frame, respectively.

The equation for the bottom volume cell 13 is given by:

$$\frac{-fK_3}{\delta x_3}T_{12}+\left[\frac{\rho_{3C_3\Delta X_3}}{\Delta t}+\frac{fK_3}{\delta x_3}\right]T_{13} \\ =f\left[h_i\left(-2\right)\right]+(1-\mathrm{f})\left[2h_i-k\frac{T_{13}-T_{12}}{\delta x_3}\right]+\frac{\rho_3 c_3 T_{13}^0\Delta x_3}{\Delta t} \tag{10}$$

3. Development of the Numerical Model

3.1. One-Phase Solution

For either completely solid or liquid PCM layers, the temperature distribution on the *n*-th layer of the wall follows the one-dimensional diffusion equation given by:

$$K_n\frac{\partial^2 T}{\partial x^2}=\rho_n c_n\frac{\partial T}{\partial t} \tag{11}$$

with the boundary condition:

$$T\left(0,t\right)=T_{\mathrm{o}}\left(t\right) \tag{12}$$

$$T\left(L,t\right)=T_l\left(t\right) \tag{13}$$

The numerical solution for a single material node yields:

$$T_i^{j+1}=T_i^j+\frac{Kn\Delta t}{\rho_n c_n\left(\Delta X\right)^2}\left(T_{i+1}^j-2T_i^j+T_{i-1}^j\right) \tag{14}$$

The finite difference equation for the inner interface is written as:

$$T_i^{j+1}=T_i^j+\frac{2\Delta t\left[K_{\mathrm{ins}}\left(T_{i-1}^j-T_i^j\right)+K_{\mathrm{pcm}}\left(T_{i+1}^j-T_i^j\right)\right]}{\left(\rho_{\mathrm{pcm}}C_{\mathrm{pcm}}+\rho_{\mathrm{ins}}C_{\mathrm{ins}}\right)\left(\Delta X\right)^2} \tag{15}$$

The finite difference equation for the outer surface is written as:

$$T_i^{j+1}=T_i^j+\frac{2\Delta t\left[K_{\mathrm{pcm}}\left(T_{i-1}^j-T_i^j\right)+K_{\mathrm{ins}}\left(T_{i+1}^j-T_i^j\right)\right]}{\left(\rho_{\mathrm{pcm}}C_{\mathrm{pcm}}+\rho_{\mathrm{ins}}C_{\mathrm{ins}}\right)\left(\Delta X\right)^2} \tag{16}$$

Depending on whether the PCM is completely solid or completely liquid upon entering the one-phase subroutine, this solution is run until the maximum nodal temperature within the PCM layer increases above the melting point or until the minimum temperature within the material drops below

the freezing point. The temperature distribution at this particular time instant becomes the initial condition for the two-phase subroutine.

3.2. Two-Phase Solution

The boundary points between the solid and liquid are held constant at the melting temperature of the material when the PCM layer consists of more than one phase and is expressed as:

$$T = T_{\mathrm{m}} \tag{17}$$

The movement of the solid-liquid boundary is given by:

$$K_{\mathrm{pcm}}[\lim_{x\to xsl+}\left(\frac{\partial T}{\partial x}\right) - \lim_{x\to xsl-}\left(\frac{\partial T}{\partial x}\right)] = \frac{\rho_{\mathrm{pcm}}\alpha \mathrm{d}_{\mathrm{xsl}}}{\mathrm{d}t} \tag{18}$$

where $xsl+$ and $xsl-$ denote the limits approaching the solid-liquid interface from the right and left, respectively.

An explicit numerical solution for a single material two-phase node is given by:

$$T_i^{j+1} = T_i^j = T_m \tag{19}$$

$$\lambda_i^{j+1} = \lambda_i^j + \frac{K_{\mathrm{pcm}}\Delta t}{\rho_{\mathrm{pcm}}\alpha\,(\Delta x)^2}(T_{i+1}^j - 2T_m + T_{i-1}^j) \tag{20}$$

where λ is the volume fraction of the i-th node, which is melted at the j-th time step. For the two PCM-insulation interface points, the finite difference equation is modified to consider that the node is half insulation and half PCM. For these two nodes, $\lambda = 1/2 = \lambda_{\max}$ indicates the fully-melted state.

For the inner interface node, the two-phase finite difference equation takes the form:

$$\lambda_i^{j+1} = \lambda_i^j + \frac{\Delta t\left[K_{\mathrm{ins}}(T_{i+1}^j - T_{\mathrm{m}}) - K_{\mathrm{pcm}}(T_{i+1}^j - T_{\mathrm{m}})\right]}{\rho_{\mathrm{pcm}}\alpha\,(\Delta x)^2} \tag{21}$$

For the outer interface node, the two-phase finite difference equation yields:

$$\lambda_i^{j+1} = \lambda_i^j + \frac{\Delta t\left[K_{\mathrm{pcm}}(T_{i+1}^j - T_{\mathrm{m}}) - K_{\mathrm{ins}}(T_{i+1}^j - T_{\mathrm{m}})\right]}{\rho_{\mathrm{pcm}}\alpha\,(\Delta x)^2} \tag{22}$$

Two-phase subroutine prepares a kind of switching between Equations (13)–(15) and Equations (15)–(18), based on the nodal state. Figure 3 shows a typical temperature for exiting the one-phase solid solution. In this case, the material is completely solid ($l = 0$) for all nodes with the outermost PCM node at some temperature slightly above T_{m}.

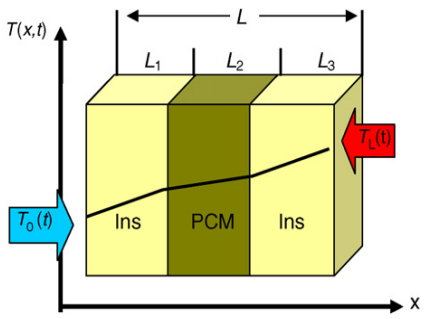

Figure 3. Typical temperature distribution for exiting the one-phase solid sub-routine.

The temperature of this node is shifted back to the PCM melting temperature and kept constant. Equation (18) is used to determine the fraction of the melted node. This is continued until l returns to zero, meaning the complete re-freezing of node or $\lambda = \lambda_{max}$, implying the complete melting of nodes. In such an instance, the temperature is again allowed to alter according to Equation (12). For the nodes that are below T_m, the temperatures are governed by the one-phase equations until they exceed T_m. At this time, the node is in two phases, and the method of calculation is toggled to Equations (15)–(18).

4. Experimental Scheme

Experiments are set up using two full-scale rooms. The test room with PCM is constructed to determine its effect on the roof and wall for thermal management of a residential building. The thermal performance of this organic eutectic PCM having a melting temperature within 40–44 °C is computed. The following criteria are satisfied for precise measurements:

(1) The PCM heat transfer is one-dimensional.
(2) The heat flow from uncontrolled outside influences is negligible compared to the applied heat.
(3) The rate of the temperature rise and fall of the PCM is comparable to reality.

The general properties of the PCM are listed in Table 1.

Table 1. PCM properties.

Properties	Value	Unit
T_m	40–44	°C
C_{ps}	2.21	kJ/kg· °C
C_{pL}	2.3	kJ/kg· °C
K_s	0.51	W/m· K
K_L	0.22	W/m· K
ρ_S	830	kg/m^3
ρ_L	878	kg/m^3
α_L	9.59×10^{-8}	m^2/s
α_S	7.92×10^{-8}	m^2/s
H	146	kJ/kg

4.1. Full-Scale Test Rooms

Two identical full-scale outdoor test rooms with dimension (3 m × 2.5 m × 2 m) as shown in Figure 4 are built at the University Technology site of Iraq. The thermal performance (internal thermal gains) of these two test rooms (PCM incorporated wall and roof) is analyzed to determine their impact under the Iraqi climate. The wall and roof of one room is covered with PCM and the other without any PCM. The basic structures (windows and supports) of both rooms are identical and made of a metallic insulated door positioned on the north wall. The thermal behavior of these rooms is compared to obtain the performance and effect of PCM. The detailed structure of these rooms is as follows:

(1) The REF is a test room without PCM. The walls (without insulation) are built using a commune brick system, cemented plaster and gypsum board. Conversely, the roof contains two layers, where the bottom slab (thickness 12 cm) is made from concrete and the top slab (thickness 10 cm) is made using a brick mixture plus mortar (Figure 4).
(2) Room 1: The structure is the same as the REF together with the incorporation of a PCM layer in the southern, eastern and western walls, as well as in the roof. The PCM (paraffin) layer is 2.5 cm thick and contained in aluminum panels (Figure 4).

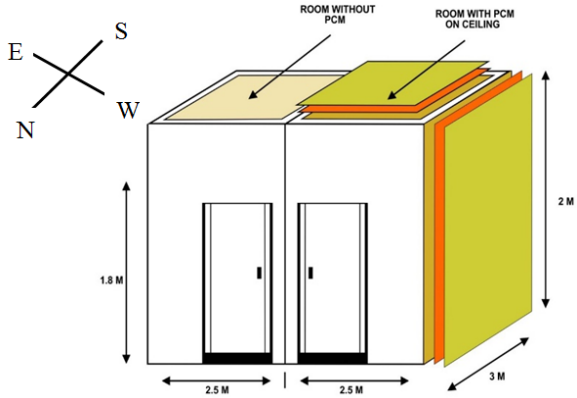

Figure 4. Geometry of the constructed test rooms, reference room (REF) (**left**, without PCM) and PCM2 (**right**).

5. Results and Discussion

Figure 5 illustrates the average variation of ambient temperature and the temperature inside the test rooms with and without PCM at a 1.5 m height in the month of August. As shown in the figure, the temperature of the room without PCM is found to increase at τ = 12 h, reaches the maximum (35 °C) between 16 h and 17 h and then decreases. This is due to the fact that initially (up to 12 h), the heat is absorbed by the room walls and roof exposed to sun and then slowly released, which caused a greenhouse-like effect of an inner increase of the temperature, as expected. Needless to say, the sun sign (solar irradiance) reaches the maximum at 12 h and remains there for a few hours before gradually dropping in later in the afternoon (beyond 17 h). On the other hand, the implementation of the PCM in the building structures reduced the room temperature peak load by 5 °C for the same time period (between 16 h and 17 h). This lowering in the peak temperature inside the room and the creation of thermal comfort is attributed to the effect of the heat storage capacity of the PCM on the temperature variation. Actually, during the first few hours of the day (up to 12 h), paraffin absorbed the latent heat from the room environment and then underwent phase transformation, thereby reducing the peak temperature. However, with the decrease of the sun sign (beyond 17 h), the latent heat is slowly released into the atmosphere. The temperature fluctuation in this case is much weaker than the one without PCM incorporated in the building. It is evident that the greenhouse effect was much lowered in the presence of PCM. This verifies the environmental friendliness of PCM when used in building management and architecture.

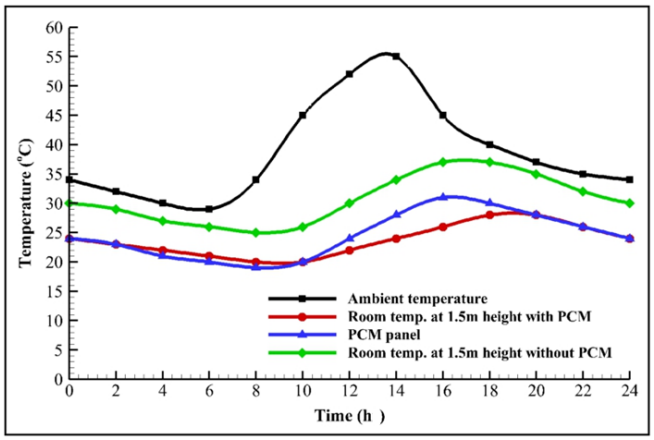

Figure 5. Temperature variation of the test rooms with and without PCM (REF) at a 1.5 m height in the month of August.

Figure 6 depicts the average variation of ambient temperature and the temperature inside the test rooms with and without PCM at a 1.5 m height in the month of January. The temperature of the room without PCM started to increase at 10 h and reached its peak load at 20 h. The temperature of the roof top reaches the maximum between 12 h and 16 h before dropping. The higher value of the roof top temperature compared to the ambient and inside ones clearly indicates the role of both radiation and convection throughout the day, as long as the sun signs; while the temperature inside the room with PCM in the winter month of January is stable all day under ambient temperature. This stability is due to the effect of using the PCM, which acts as a heat storage capacitor and diminishes the rapid temperature fluctuation via phase transformation. During phase conversion in paraffin, a huge amount of latent heat exchange occurs at a constant temperature. This elevated absorption of heat by the PCM materials is indeed responsible for the reduction of the heat flux inside the room and the maintenance of thermal comfort. Specifically, the use of PCM in the building walls and roof increased their thermal resistance and thereby reduced the overall heat transfer through the walls with much lowered heat load compared to the building without PCM.

The temperature variation for the PCM and non-PCM walls is theoretically examined. The east, south and west walls are used to calculate the heat flux through the external and internal walls' surface and the amount of heat storage in the walls. In Figures 7–9 the external heat flux, heat storage and internal heat flux on the east wall of both types of rooms have been compared. Figure 9 (heat flux through the external wall) clearly reveals that the heat flux for the PCM incorporated room is slightly higher than the one without PCM on the walls. This observation is attributed to the low thermal conductivity of the liquid PCM, which reduced the heat transmission to the room and thereby increased the wall top surface temperature. The maximum value of heat flux through the PCM including and excluding the external wall at 9 h is found to be 312 W/m^2 and 162 W/m^2, respectively. Conversely, the heat flux (at 21.5 h) through the internal east wall of the room with and without PCM is discerned to be 26 W/m^2 and 44 W/m^2, respectively. Furthermore, heat storage is observed to be maximum at 12 h with values of 240 W/m^2 and 135 W/m^2 for the PCM integrated and non-integrated east walls, respectively.

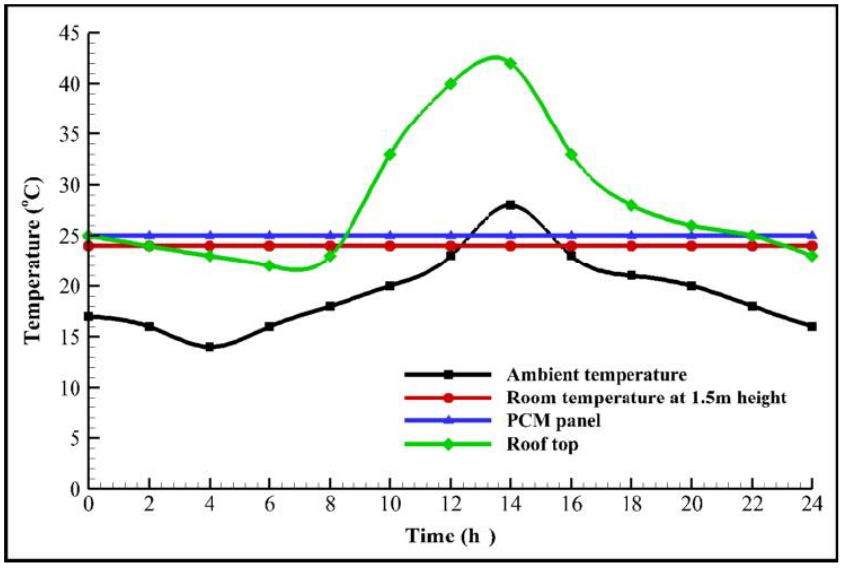

Figure 6. Temperature variation of the test room with and without PCM (REF) at a height of 1.5 m in the month of January.

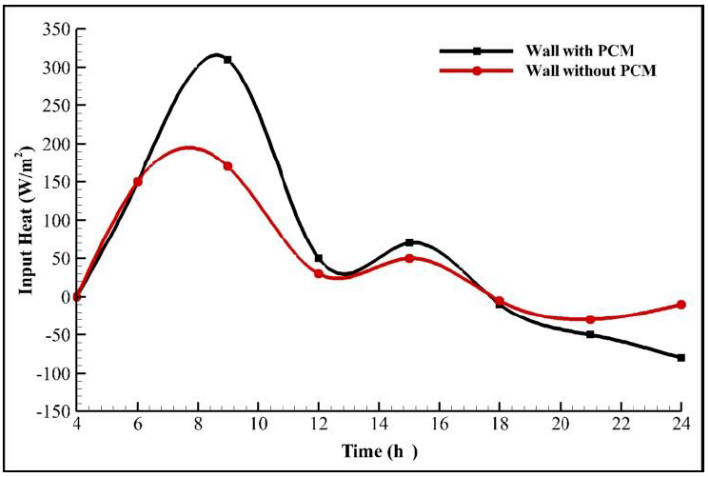

Figure 7. Heat flux through the external surface of the non-PCM- and PCM-treated east walls.

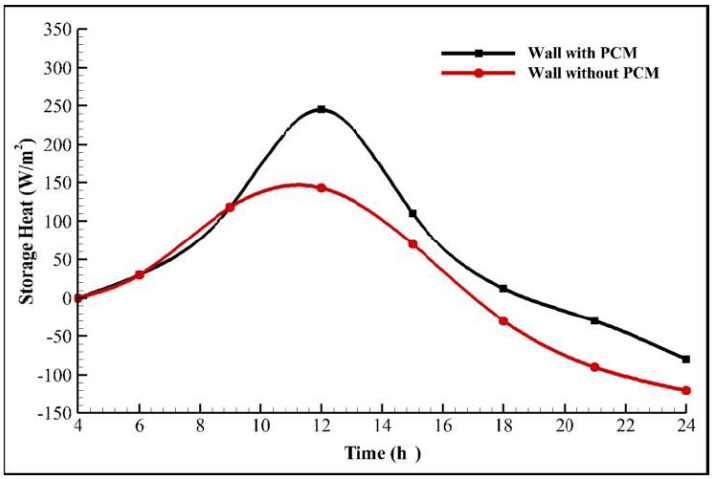

Figure 8. Amount of heat storage in the non-PCM- and PCM-treated east walls.

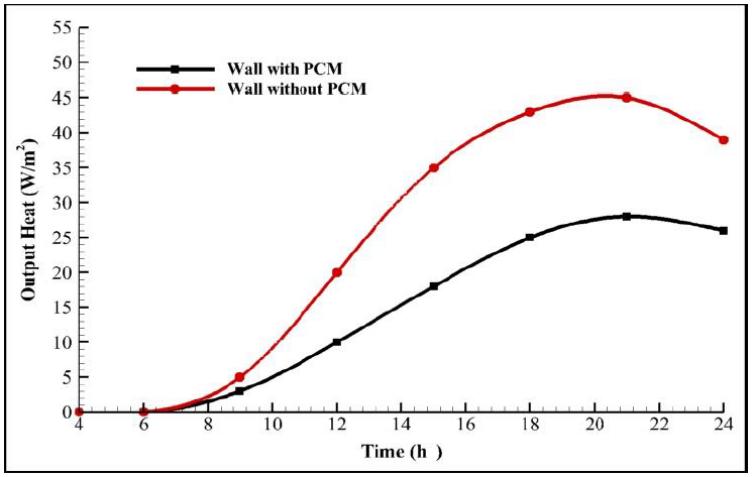

Figure 9. Heat flux through the internal surface of the non-PCM- and PCM-treated east walls.

The variation of heat flux and storage for the south and west walls for the rooms with and without the incorporation of PCM is demonstrated in Figures 10–15. These variations in heat and storage profiles are similar to those of the east wall.

The value of thermal flow and heat storage through a selected wall is computed using finite volume method (FVM), where the thermal flow (through the wall for both the internal and external surface) is calculated. A fixed value of the internal and external heat transfer coefficient is used, which is 7.73 $W/m^2 \cdot {}^\circ C$ and 23.3 $W/m^2 \cdot {}^\circ C$ for the internal and external wall surface, respectively. The amount of stored heat in the walls containing PCMs is found to be larger than the traditional (REF) walls. This elevated storage in PCM walls is ascribed to the high heat capacity and heat-retaining susceptibility without connecting any storage space to the air conditioner. The observed higher thermal storage for the western walls is related to the longest exposure to the solar radiation.

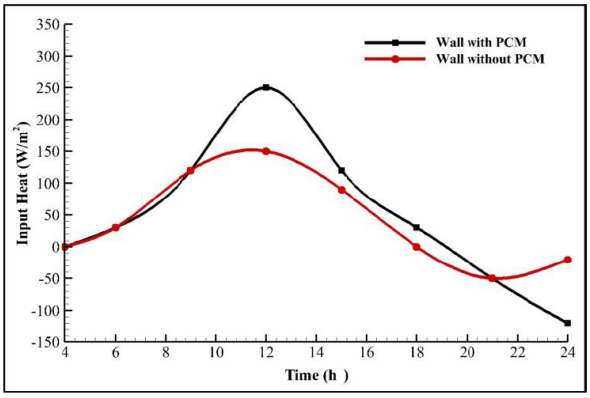

Figure 10. Heat flux through the external surface of the non-PCM- and PCM-treated south walls.

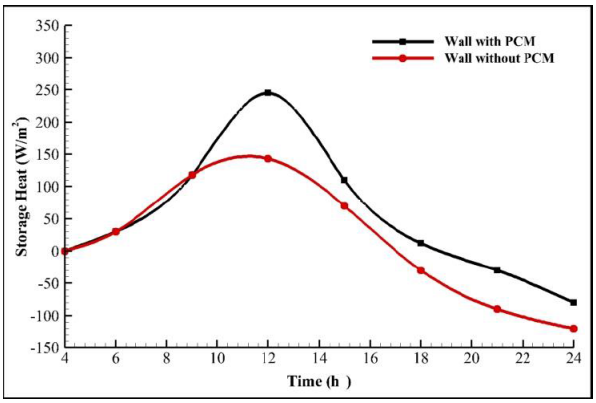

Figure 11. Amount of heat storage of the non-PCM- and PCM-treated south walls.

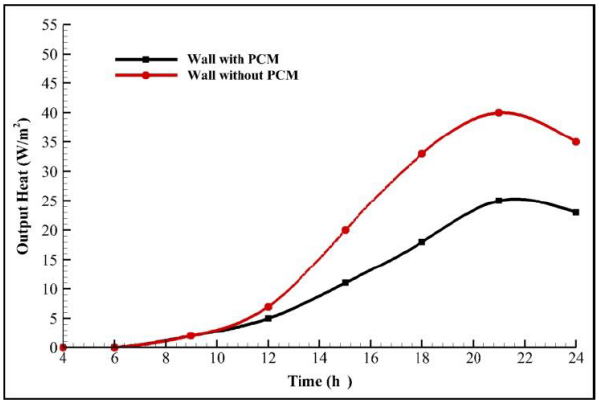

Figure 12. Heat flux through the internal surface of the non-PCM- and PCM-treated south walls.

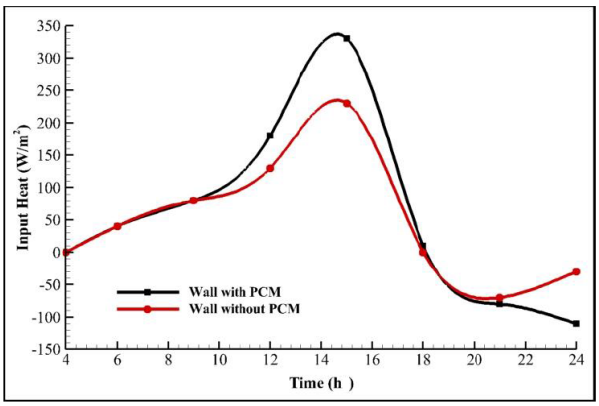

Figure 13. Heat flux through the external surface of the non-PCM- and PCM-treated west walls.

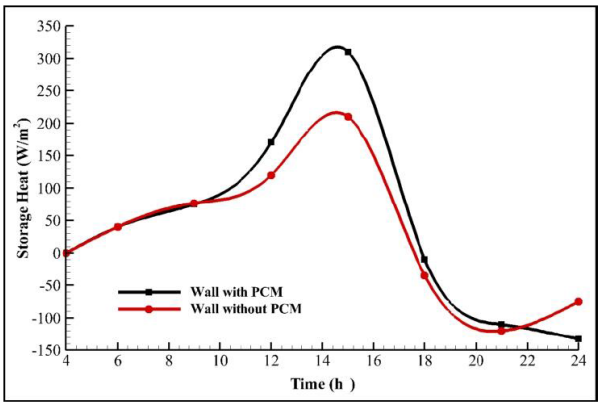

Figure 14. Amount of heat storage in the non-PCM- and PCM-treated west walls.

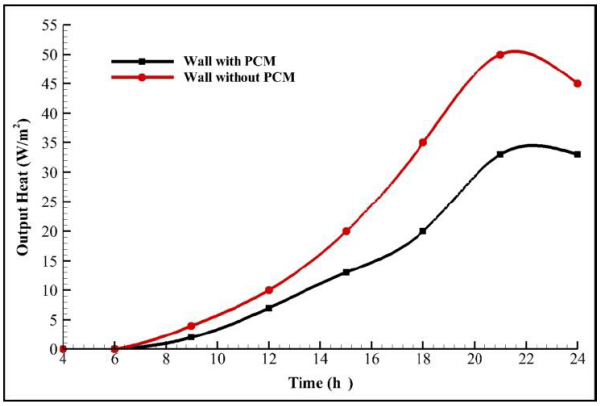

Figure 15. Heat flux through the internal surface of the non-PCM- and PCM-treated west walls.

The simulated temperature contours for REF and PCM2 at different times over the day are illustrated in Figures 16–19. It is evident that the room with PCM integration in the roof achieves a superior temperature distribution throughout the day than the one without PCM. However, with the increase of sun sign, the temperature fluctuation became more prominent (at 12 h) for the REF room, as shown in Figure 20a. The temperature fluctuation kept on increasing at 16 h and 18 h, as depicted in Figures 21a and 22a.

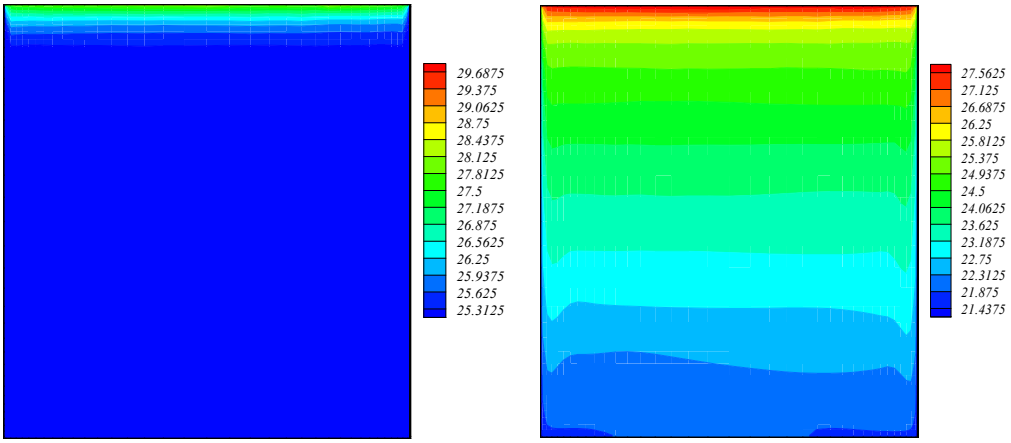

Figure 16. Temperature counters of the roof at 8 h for the room: (**a**) without and (**b**) with PCM.

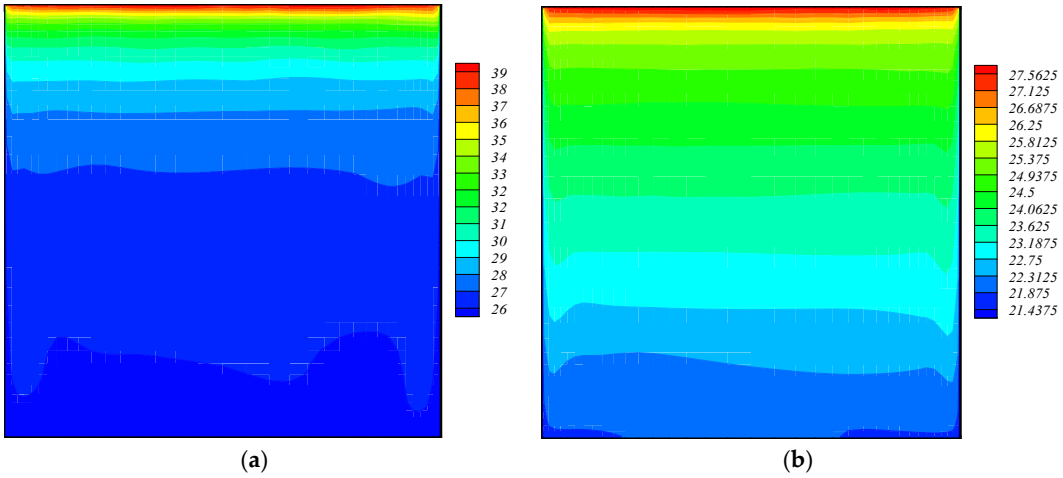

Figure 17. Temperature counters of the roof at 12 h for the room: (**a**) without and (**b**) with PCM.

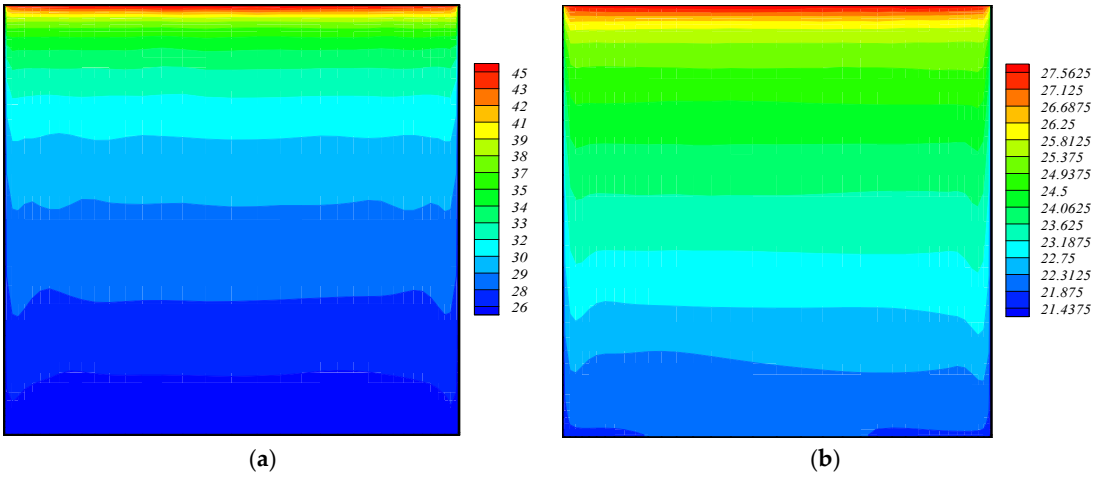

Figure 18. Temperature counters of the roof at 16 h for the room: (**a**) without and (**b**) with PCM.

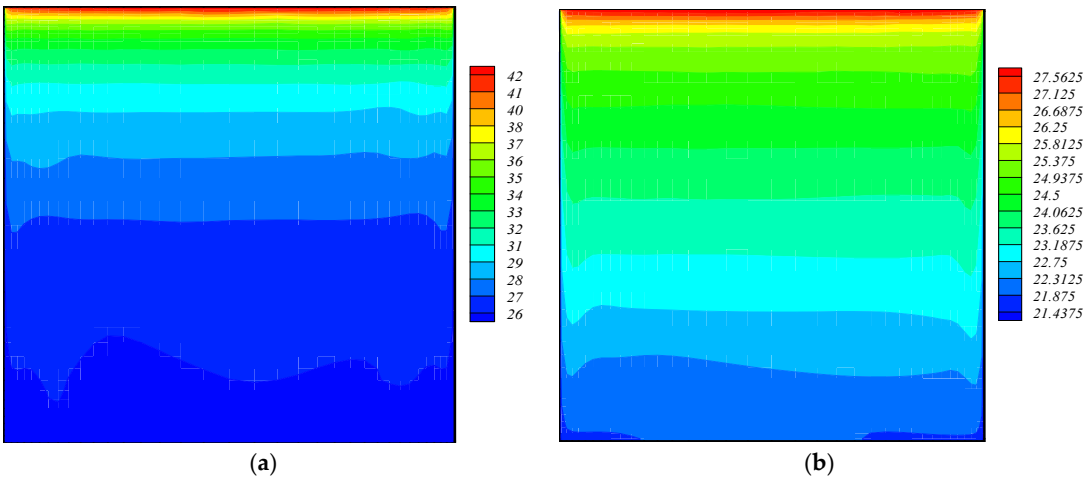

Figure 19. Temperature counters of the roof at 18 h for the room (**a**) without and (**b**) with PCM.

Figures 20 and 21 compare the simulation and experimental results of the roof temperature for the rooms with and without PCM, respectively.

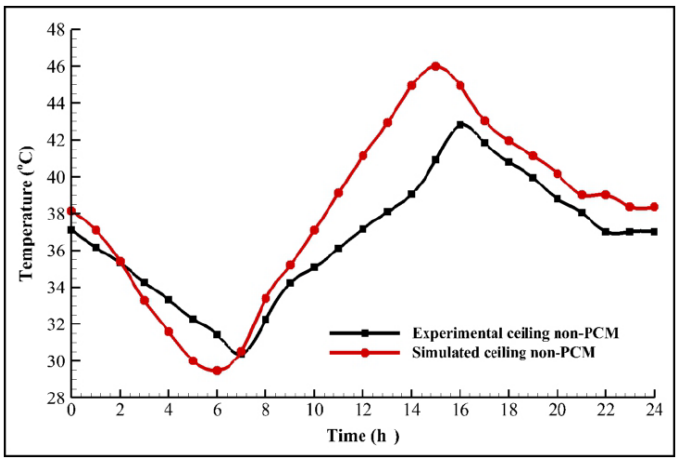

Figure 20. Experimental and simulated temperature of the PCM integrated roof.

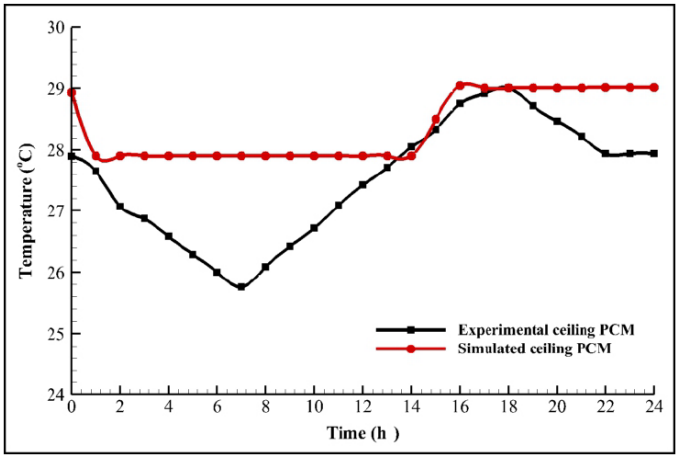

Figure 21. Experimental and simulated temperature of the REF roof.

It is evident that the ceiling (concrete) temperature of the room containing PCM maintained the temperature constant (27 °C) throughout the day as compared to that of the conventional room. This demonstrates that the environment insignificantly affects the inner surface of the ceiling, because all of the heat energy is absorbed by the PCM installed in the roof. Conversely, a considerable temperature fluctuation is observed in the ceiling of the REF (without PCM), because the outside environment immediately influenced its ceiling. Furthermore, the experimental results for PCM2 revealed a small reduction in ceiling temperature during the day time and slight augmentation during the night time. This diminished temperature fluctuation of PCM2 arose from the large heat storage capacity of the PCM. The occurrence of the observed temperature differences between the simulation and experimental results is ascribed to the following reasons:

(1) The room ceiling is influenced by interior condition, where an actual temperature variation occurred.
(2) The effective thermal conductivity of the PCM in the experiment is higher due to the presence of uniformly-distributed high conductivity heat exchanger material in the PCM panel.
(3) The actual phase change may not occur during the phase change temperature as prescribed in the theory.

Figure 22 shows the simulated heat flux entering the room. It is clear that the PCM incorporated roof is better than the one without PCM. The implementation of PCM in the building structure remarkably reduced (more than two-thirds) the heat entry compared to the room without PCM integration. Moreover, the presence of PCM reduced the heat transfer by 46.71% which is directly proportional to reduction in the electricity consumption to maintain the room at 25 °C. Hence, the incorporation of PCM in the building architecture of Iraq is recommended because of thermal comfort, cost-effectiveness and environmental friendliness.

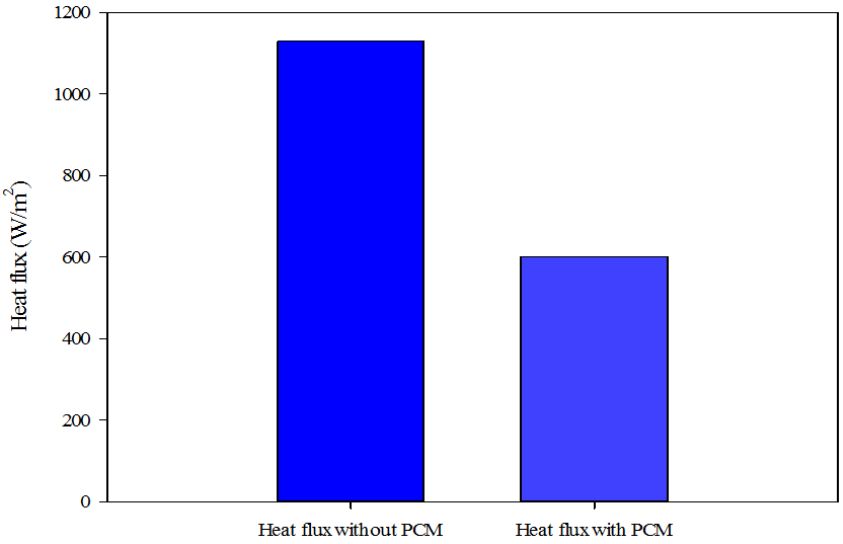

Figure 22. The simulated heat flux entering the room.

6. Conclusions

Thermal management of locally-extracted PCM (paraffin with 40% oil and 60% wax) incorporated building structures in the specific climatic condition of Iraq is reported. Experiments and numerical investigations are made to examine the heat flux reduction inside a residential building using such PCMs. These inexpensive PCMs are obtained from waste petroleum products in Iraq. Two rooms of identical internal dimensions are built, one with PCM and the other without PCM in the roof and walls. The thermal performances of these full-scale test rooms are evaluated. The experimental

results are complemented using two-dimensional numerical transient heat transfer (laminar and turbulent flows) model simulation, where the finite difference method is used to solve the discretized equations. The computations are conducted to obtain the solution of heat transfer in a square cavity with differentially-heated side walls. Simulation and experimental results revealed a good agreement. The heat flux inside the PCM integrated room is demonstrated to be considerably lower than the one without PCM. The admirable features of the results suggest that our systematic theoretical and simulation studies may contribute towards the development of thermal management of PCM integrated buildings in Iraq.

Acknowledgments: The authors would like to thank the Ministry of Science, Technology and Innovation (MOSTI) and the Universiti Teknologi Malaysia for supporting this research activity under a science grant under Grant Research No. R.J130000.7924.4S080. The authors are grateful to the staff of the Department of Mechanical Engineering, University of Technology-Iraq, for their help. Hussein is grateful to the government of Iraq for providing the financial support and study leave to complete the doctoral degree.

Author Contributions: The contributions of each author are as follows: Hussein J. Akeiber and Seyed Ehsan Hosseini provided the impetus for this work and analyzed the experimental and numerical results and drafted the manuscript. Mazlan A. Wahid, Hasanen M. Hussen and Abdulrahman Th. Mohammad provided insights that led to highlighting some of the distinctions between equations and worked on rewrites and clarifications. All authors have read and approved the final manuscript.

Conflicts of Interest: The authors declare no conflict of interest.

Nomenclatures

C_1, C_3	Specific heat of roof top slab and concrete slab (kJ/kg· K)
C_{pl}	Specific heat of liquid PCM (kJ/kg· K)
C_{ps}	Specific heat of solid PCM (kJ/kg· K)
f	Implicit factor
$\mathrm{Gr_L}$	Grashof number
h_{i}	Inside heat transfer coefficient (W/m^2· K)
h_{o}	Outside heat transfer coefficient (W/m^2· K)
k_1, k_2, k_3	Thermal conductivity of roof top slab, PCM panel and bottom concrete slab (W/m· K)
L_1, L_2, L_3	Thickness of roof top slab, PCM panel and bottom concrete slab (m)
$\mathrm{Nu_L}$	Nusselt number
P_{r}	Prandtl number
q_{rad}	Radiation flux (W/m^2)
Re	Reynolds number
T	Temperature
T_∞	Ambient temperature
T_i^0	Previous time step temperature at i-th volume cell
T_i	Current time step temperature at i-th volume cell
T_{in}	Initial temperature
T_{room}	Room temperature
T_{s}	Surface temperature
T_{sky}	Sky temperature
α	Absorptivity
ε	Emissivity
h_{sl}	Solid-liquid enthalpy change (kJ/kg)
σ	Stefan-Boltzmann constant
ρ_1, ρ_2, ρ_3	Density of roof top slab, PCM panel and bottom concrete slab (kg/m^3)
Δt	Time step (s)
δx_1, δx_2, δx_3	Nodal distances (m)
Δx_1, Δx_2, Δx_3	Control volume length of roof top slab, PCM panel and bottom concrete slab (m)

References

1. Tenorio, J.A.; Sánchez-Ramos, J.; Ruiz-Pardo, Á.; Álvarez, S.; Cabeza, L.F. Energy Efficiency Indicators for Assessing Construction Systems Storing Renewable Energy: Application to Phase Change Material-Bearing Façades. *Energies* **2015**, *8*, 8630–8649. [CrossRef]
2. Lo Brano, V.; Ciulla, G.; Piacentino, A.; Cardona, F. On the efficacy of PCM to shave peak temperature of crystalline photovoltaic panels: An FDM model and field validation. *Energies* **2013**, *6*, 6188–6210. [CrossRef]
3. Seong, Y.B.; Lim, J.H. Energy Saving Potentials of Phase Change Materials Applied to Lightweight Building Envelopes. *Energies* **2013**, *6*, 5219–5230. [CrossRef]
4. Normura, T.; Tsubota, M.; Oya, T.; Okinka, N.; Akiyama, T. Heat storage in direct-contact heat exchanger with phase change material. *Appl. Therm. Eng.* **2013**, *50*, 26–34. [CrossRef]
5. Oro, E.; De Gracia, A.; Castell, A.; Farid, M.M.; Cabeza, L.F. Review on phase change materials (PCMs) for cold thermal energy storage applications. *Appl. Energy* **2012**, *99*, 513–533. [CrossRef]
6. Rezaei, M.; Anisur, M.R.; Mahfuz, M.H.; Kibria, M.A.; Saidur, R.; Metselaar, I.H.S.C. Performance and cost analysis of phase change materials with different melting temperatures in heating system. *Energy* **2013**, *5*, 173–178. [CrossRef]
7. Li, Y.; Zhang, Y.; Li, M.; Zhang, M. Testing method of phase change temperature and heat of inorganic high temperature phase change materials. *Exp. Therm. Fluid Sci.* **2013**, *44*, 697–707. [CrossRef]
8. Romero-Sanchez, M.D.; Guillem-Lopez, C.; Lopez-Buendia, A.M.; Stamatiadou, M.; Mandilaras, I.; Katsourinis, D.; Founti, M. Treatment of natural stones with phase change materials: Experiments and computational approaches. *Appl. Therm. Eng.* **2012**, *48*, 136–143. [CrossRef]
9. Izquierdo-Barrientos, M.A.; Belmonte, J.F.; Rodríguez-Sánchez, D.; Molina, A.E.; lmendros-Ibáñez, J.A. A numerical study of external building walls containing phase change materials (PCM). *Appl. Therm. Eng.* **2012**, *47*, 73–85. [CrossRef]
10. Kuznik, F.; Virgone, J. Experimental assessment of a phase change material for wall building use. *Appl. Energy* **2009**, *86*, 2038–2046. [CrossRef]
11. De Gracia, A.; Rincón, L.; Castell, A.; Jiménez, M.; Boerb, D.; Medrano, M.; Cabez, L.F. Life Cycle Assessment of the inclusion of phase change materials (PCM) in experimental buildings. *Energy Build.* **2010**, *42*, 1517–1523. [CrossRef]
12. Kuznik, F.; Virgone, J.; Noel, J. Optimization of a phase change material wallboard for building use. *Appl. Therm. Eng.* **2008**, *28*, 1291–1298. [CrossRef]
13. Navarro, L.; de Garcia, A.; Solé, C.; Castell, A.; Cabeza, L.F. Thermal loads inside buildings with phase change materials: Experimental results. *Energy Proced.* **2012**, *30*, 342–349. [CrossRef]
14. Pasupathy, A.; Velraj, R. Effect of double layer phase change material in building roof for year round thermal management. *Energy Build.* **2008**, *40*, 193–203. [CrossRef]